Faraday Discussions

Accepted Manuscript

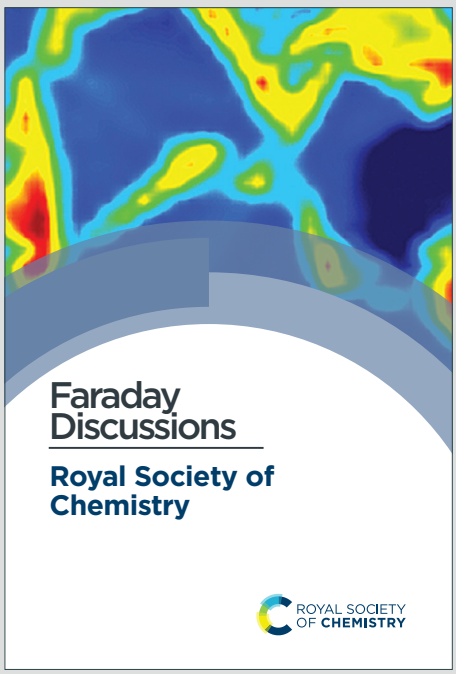

This article can be cited before page numbers have been issued, to do this please use: J. Ha, E. Leal-Sánchez and R. J. MacDonell, *Faraday Discuss.*, 2026, DOI: 10.1039/D6FD00096G.

ROYAL SOCIETY OF CHEMISTRY

www.rsc.org/faraday_d

View Article Online
DOI: 10.1039/D6FD00096G

Towards direct dynamics simulation of photochemistry without the Born-Oppenheimer approximation

Jong-Kwon Ha,[a] Edith Leal-Sánchez[a] and Ryan J. MacDonell*[ab]

Received 00th January 20xx, Accepted 00th January 20xx DOI: 10.1039/x0xx00000x

The simulation of photochemical reactions requires a quantum mechanical treatment of electronic and nuclear dynamics. Most simulation approaches use the Born-Oppenheimer (BO) approximation and calculations of nonadiabatic couplings to evolve a wavefunction on a set of BO electronic states. However, the use of BO states present several challenges such as discontinuous surfaces, singular terms in the Hamiltonian, and double-valued boundary conditions. We present a direct dynamics approach for molecular vibronic dynamics which does not invoke the BO approximation simply by avoiding diagonalization of the electronic part of the Hamiltonian. By employing a diabatic propagation scheme for the orbitals, we ensure that all electronic terms vary smoothly as a function of nuclear coordinates in a basis of configuration state functions (CSFs). We derive equations of motion for mixed quantum-classical dynamics techniques employing averaged potentials, such that the simulated trajectories evolve on linear combinations of CSF surfaces. We test our approach for lithium hydride and ethylene. In contrast with BO electronic surfaces, we find that all CSF surfaces and couplings are smooth and integrable in the vicinity of conical intersections and weak avoided crossings. Comparisons of the dynamics of photoexcited lithium hydride show that Ehrenfest dynamics reproduce changes in electronic state populations, but lead to over-coherence. Our equations of motion for coupled-trajectory dynamics fail to reduce the over-coherence problem due to the reliance of the derivation on the BO approximation. With further work on the selection of orbitals and the mixed quantum-classical equations of motion, our work shows the potential of a pre-BO wavefunction ansatz for practical nonadiabatic dynamics simulations.

1 Introduction

Photochemical reactions involve the excitation of electronic states by the absorption of light, and the subsequent dispersal of the electronic energy. Understanding their mechanism is important for the comprehension of biological processes, such as vision and photosynthesis[1–3], as well as for developing new materials such as those with photovoltaic or photochromic properties[4–8]. Time-resolved spectroscopic techniques have revealed that the coupling between electronic and nuclear motion play a crucial role in photochemical reactions[9–12]. However, the most common approaches in quantum chemistry use the Born-Oppenheimer (BO) approximation, which neglects the coupling of electronic states due to nuclear motion[13–16]. Simulations of photochemical reactions thus have the added challenge of overcoming or correcting the BO approximation.

[a] Department of Chemistry, Dalhousie University, 6243 Alumni Cres, Halifax, NS B3H 4R2, Canada
[b] Department of Physics and Atmospheric Science, Dalhousie University, 1493 Lord Dalhousie Dr, Halifax, NS B3H 4R2, Canada; E-mail: rymac@dal.ca

[0]† Supplementary Information available: LiH CSF and BO energies, LiH initial positions and momenta, ethylene optimized MECI geometry, ethylene g and h vectors, ethylene orthonormalized g and h vectors. See DOI: 00.0000/00000000.

View Article Online
DOI: 10.1039/D6FD00096G

Methods used to simulate photochemical reactions are collectively known as nonadiabatic dynamics methods due to their correction of the BO (adiabatic) ansatz. A full quantum mechanical treatment of nuclear degrees of freedom is only achievable for small molecules, or simplified models of molecular Hamiltonians[17,18]. Nonetheless, a full quantum mechanical treatment can accurately predict short-time observables such as vibronic spectra for certain molecules using fitted Hamiltonians and numerically efficient approaches such as multiconfigurational time-dependent Hartree[19,20]. To avoid the up-front cost of fitting Hamiltonians, direct dynamics methods use only local information to propagate an approximate wavefunction. One class of direct dynamics methods are mixed quantum-classical (MQC) methods, which use classical equations of motion to propagate trajectories in nuclear coordinate space[21]. Methods such as trajectory surface hopping (TSH) and Ehrenfest dynamics (Eh) require much less computational resources than their fully quantum mechanical counterparts[22–26]. However, they lack nuclear quantum effects and typically introduce over-coherence of the electronic states. Several corrections have been formulated to overcome the over-coherence problem of MQC methods[27–30].

The majority of nonadiabatic dynamics methods rely on calculations involving the BO approximation due to the widespread accessibility of BO-based electronic structure methods. BO-based methods use the eigenstates of the electronic Hamiltonian as an electronic state basis. Consequently, the electron-nuclear couplings appear as derivative couplings between the nuclear momentum and the electronic wavefunction[13,16]. A full treatment of the Hamiltonian also includes second-order couplings, which are very challenging to compute and are often neglected. The derivative couplings in the BO basis are singular at subspaces of the nuclear coordinate space known as conical intersections, where two (or more) electronic states are degenerate. Conical intersections appear as cusps in the potential energy surfaces, and a BO wavefunction encircling a conical intersection acquires a geometric phase with double-valued boundary conditions[9,13,31,32]. These characteristics make simulations with BO-based methods challenging and typically require additional approximations.

In contrast, pre-BO ansätze avoid employing the BO approximation from the outset by treating electrons and nuclei on the same footing. For example, grid-based methods can simulate electrons and nuclei together on a multidimensional grid at an exponential computational cost. Other methods reduce the cost by reducing the basis size, for example by employing Gaussian basis sets depending on correlated degrees of freedom[33,34], or by defining single-particle functions for nuclei akin to electronic orbitals[35,36]. Recently, a new framework for pre-BO approaches was proposed in which the electronic degrees of freedom are quantized in an electronic orbital basis with coefficients depending on nuclear coordinates[37,38]. The nuclear degrees of freedom can be subsequently quantized and truncated at a low order[37,39]. By choosing a basis where the electronic orbitals vary slowly with nuclear coordinates, these methods offer the potential for highly accurate calculations of photochemical properties and dynamics.

The definition of an electronic basis which avoids the problems associated with BO-based methods is by no means a new problem. A diabatic electronic basis is one in which derivative couplings vanish, which has been proven to be non-existent for a finite number of electronic states[40–42]. Quasi-diabatic bases instead assume that derivative couplings become negligible where potential energies and couplings are smooth functions of nuclear coordinates.[43] Such approaches are typically fitted to reproduce BO-based potentials or other properties[13,44]. Similarly, the adoption of "diabatic orbitals" is known to produce slowly varying Hamiltonians in a many-body electronic basis. The diabatization of orbitals is generally achieved using unitary transformations between orbitals at adjacent nuclear geometries[45], and optimization of the orbitals and their transformations have led to robust techniques for the

View Article Online
DOI: 10.1039/D6FD00096G

preparation of quasi-diabatic molecular Hamiltonians[43,46–48].

An alternate view of photochemical dynamics arises from the use of the exact factorization formalism. It exactly factorizes the time-evolving molecular wavefunction as a single product of time-evolving electronic and nuclear wavefunctions[49,50]. The formalism introduces a new starting point for nonadiabatic dynamics methods. It has led to the development of alternate quantum mechanical[51] and MQC[52–58] approaches based on the concept of a time-evolving potential energy surface and an electron-nuclear correlation (ENC) operator. The MQC approaches include terms originating from the ENC operator, which correct for over-coherence in the BO basis through the derivation of a collective force that acts between trajectories[52–58] as well as corrections to phase evolution[58]. Exact factorization has been applied primarily to develop new BO-based nonadiabatic dynamics methods, but it is equally applicable to any form of the molecular wavefunction.

In this paper, we take the first steps toward a direct dynamics methodology which simulates photochemical dynamics with a pre-BO ansatz. We derive the full set of terms in the molecular Hamiltonian with an orbital basis as well as a method to smoothly propagate the orbitals with or without an active space. We propose an MQC approximation to the dynamics based on exact factorization. We test our approach by preparing the elements of the Hamiltonians of lithium hydride and ethylene, and by simulating exact and MQC dynamics of lithium hydride. Finally, we conclude by offering paths for improvement to the selection of basis and MQC equations of motion. Our results show the promise of a pre-BO ansatz for direct dynamics simulation at an affordable computational cost.

2 Theory

2.1 Quantum molecular dynamics

The molecular Hamiltonian can be written in terms of the nuclear kinetic energy and the Born-Oppenheimer electronic Hamiltonian, $\hat{H}_{\mathrm{mol}} = \hat{T}_{\mathrm{n}} + \hat{H}_{\mathrm{e}}$, given by

$$\hat{T}_{\mathrm{n}} = -\sum_{\nu}^{N_{\mathrm{n}}} \frac{1}{2M_\nu} \boldsymbol{\nabla}_\nu^2, \tag{1}$$

$$\hat{H}_{\mathrm{e}} = -\frac{1}{2}\sum_{i}^{N_{\mathrm{e}}} \left(\boldsymbol{\nabla}_i^2 + \sum_{\nu}^{N_{\mathrm{n}}} \frac{Z_\nu}{|\mathbf{r}_i - \mathbf{R}_\nu|} \right) + \sum_{i>j}^{N_{\mathrm{e}}} \frac{1}{|\mathbf{r}_i - \mathbf{r}_j|} + V_{\mathrm{nn}}, \tag{2}$$

$$V_{\mathrm{nn}} = \sum_{\nu>\mu}^{N_{\mathrm{n}}} \frac{Z_\nu Z_\mu}{|\mathbf{R}_\nu - \mathbf{R}_\mu|}, \tag{3}$$

where N_{e} is the number of electrons, $\mathbf{r}_i$ is the position of electron i, $\boldsymbol{\nabla}_i$ is its gradient, N_{n} is the number of nuclei, $\mathbf{R}_\nu$ is the position of nucleus ν, $\boldsymbol{\nabla}_\nu$ is its gradient, Z_ν is its charge, and M_ν is its mass. We use atomic units ($\hbar = m_{\mathrm{e}} = e = 4\pi\varepsilon_0 = 1$) here and throughout this paper.

The molecular wavefunction can be written as

$$\Psi_{\mathrm{mol}}(\mathbf{r}, \mathbf{R}, t) = \sum_I \chi_I(\mathbf{R}, t) \Phi_I(\mathbf{r}; \mathbf{R}) \tag{4}$$

with a basis of many-body electronic states $\Phi_I(\mathbf{r};\mathbf{R})$ and nuclear wavefunctions $\chi_I(\mathbf{R},t)$ projected on each state I, where $\mathbf{R} = \begin{pmatrix} \mathbf{R}_1^{\mathsf{T}} & \mathbf{R}_2^{\mathsf{T}} & \cdots & \mathbf{R}_{N_{\mathrm{n}}}^{\mathsf{T}} \end{pmatrix}^{\mathsf{T}}$ is a vector of all nuclear coordinates. With this wavefunction ansatz, the kinetic energy leads to nonadiabatic coupling terms because $\boldsymbol{\nabla}_\nu$ acts on the electronic basis. We define a left-acting gradient operator $\boldsymbol{\nabla}_\nu^\dagger = -\boldsymbol{\nabla}_\nu^{\mathsf{T}}$ which accounts for its anti-Hermiticity, and we expand the kinetic energy into matrix elements of the many-body electronic

View Article Online
DOI: 10.1039/D6FD00096G

basis

$$\begin{aligned}\mathbb{T}_{n,IJ} &= \sum_{\nu} \frac{1}{2M_\nu} \langle \Phi_I | \boldsymbol{\nabla}_\nu^\dagger \boldsymbol{\nabla}_\nu | \Phi_J \rangle_{\mathbf{r}} \\ &= \sum_{\nu} \frac{1}{2M_\nu} \left(\boldsymbol{\nabla}_\nu^\dagger \langle \Phi_I | \Phi_J \rangle_{\mathbf{r}} \boldsymbol{\nabla}_\nu + \boldsymbol{\nabla}_\nu^\dagger \langle \Phi_I | \boldsymbol{\nabla}_\nu \Phi_J \rangle_{\mathbf{r}} + \langle \boldsymbol{\nabla}_\nu \Phi_I | \Phi_J \rangle_{\mathbf{r}} \boldsymbol{\nabla}_\nu + \langle \boldsymbol{\nabla}_\nu \Phi_I | \boldsymbol{\nabla}_\nu \Phi_J \rangle_{\mathbf{r}} \right) \\ &= \sum_{\nu} \frac{1}{2M_\nu} |\boldsymbol{\nabla}_\nu + \mathbf{D}_{\nu,IJ}|^2 + G_{IJ}, \end{aligned} \tag{5}$$

where $|\Phi_I\rangle$ is the state vector of $\Phi_I(\mathbf{r};\mathbf{R})$, the subscript $\mathbf{r}$ denotes integration over electronic coordinates, and $|\cdot|^2$ is the square modulus. The resulting equation contains a vector and scalar potential given by

$$\mathbf{D}_{\nu,IJ} = \langle \Phi_I | \boldsymbol{\nabla}_\nu \Phi_J \rangle_{\mathbf{r}}, \tag{6}$$

$$G_{IJ} = \sum_{\nu} \frac{1}{2M_\nu} \langle \boldsymbol{\nabla}_\nu \Phi_I | \left(1 - \sum_K |\Phi_K\rangle \langle \Phi_K| \right) | \boldsymbol{\nabla}_\nu \Phi_J \rangle_{\mathbf{r}}. \tag{7}$$

In the complete electronic basis limit, G_{IJ} vanishes because it involves the projection into the orthogonal complement of the basis.

Using the definitions above, the molecular Hamiltonian is expressed as a matrix in the many-electron basis by

$$\mathbb{H}_{\mathrm{mol}} = \langle \Phi | \hat{H}_{\mathrm{mol}} | \Phi \rangle_{\mathbf{r}}^{\mathsf{T}} = \sum_{\nu} \frac{1}{2M_\nu} |\boldsymbol{\nabla}_\nu + \mathbb{D}_\nu|^2 + \mathbb{V}, \tag{8}$$

where $|\Phi\rangle$ is a vector with elements $|\Phi_I\rangle$, $\mathbb{D}_\nu$ is a matrix of vectors with elements $\mathbf{D}_{\nu,IJ}$, and $\mathbb{V} = \mathbb{H}_{\mathrm{e}} + \mathbb{G}$ is the potential energy matrix with $\mathbb{H}_{\mathrm{e}} = \langle \Phi | \hat{H}_{\mathrm{e}} | \Phi \rangle_{\mathbf{r}}^{\mathsf{T}}$ with elements $[\mathbb{H}_e]_{IJ} = H_{e,IJ}$ and $[\mathbb{G}]_{IJ} = G_{IJ}$. As a result, the molecular dynamics are described by coupled differential equations for nuclear wavefunctions evolving on electronic states

$$i\frac{\partial}{\partial t} \chi(\mathbf{R},t) = \mathbb{H}_{\mathrm{mol}} \chi(\mathbf{R},t), \tag{9}$$

where $\chi(\mathbf{R},t)$ is a vector with elements $\chi_I(\mathbf{R},t)$.

2.2 Second quantization representation

Using electronic creation and annihilation operators ($\hat{a}_p^\dagger$ and $\hat{a}_p$, respectively, for orbital p), the elements of $\mathbb{H}_{\mathrm{mol}}$ are given by

$$\mathbb{H}_{\mathrm{e}} = \sum_{pq}^{N_{\mathrm{o}}} h_q^p(\mathbf{R}) \langle \Phi | \hat{a}_p^\dagger \hat{a}_q | \Phi \rangle^{\mathsf{T}} - \frac{1}{2} \sum_{pqrs}^{N_{\mathrm{o}}} v_{rs}^{pq}(\mathbf{R}) \langle \Phi | \hat{a}_p^\dagger \hat{a}_q^\dagger \hat{a}_r \hat{a}_s | \Phi \rangle^{\mathsf{T}} + V_{\mathrm{nn}}(\mathbf{R}), \tag{10}$$

$$\mathbb{D}_\nu = \sum_{pq}^{N_{\mathrm{o}}} \mathbf{d}_{q,\nu}^p(\mathbf{R}) \langle \Phi | \hat{a}_p^\dagger \hat{a}_q | \Phi \rangle^{\mathsf{T}}, \tag{11}$$

$$\mathbb{G} = \sum_{pq}^{N_{\mathrm{o}}} g_q^p(\mathbf{R}) \langle \Phi | \hat{a}_p^\dagger \hat{a}_q | \Phi \rangle^{\mathsf{T}}, \tag{12}$$

where N_{o} is the number of orbitals, $|\Phi\rangle$ is a vector of many-body electronic states which can be written as linear combinations of configuration state functions (CSFs), and the nuclear position dependence is expressed by a set of one- and two-electron integrals $h_q^p(\mathbf{R})$, $v_{rs}^{pq}(\mathbf{R})$, $\mathbf{d}_{q,\nu}^p(\mathbf{R})$, and $g_q^p(\mathbf{R})$.

In what follows, we consider the case where spin-orbit coupling is negligible and there are no external electric or magnetic fields. The generalization is straightforward but requires additional terms and a larger electronic basis. Without spin-orbit

View Article Online
DOI: 10.1039/D6FD00096G

coupling, the integrals are given by

$$h_q^p(\mathbf{R}) = \delta_{\sigma_p\sigma_q}\tilde{h}_q^p(\mathbf{R}) = -\delta_{\sigma_p\sigma_q}\int \mathrm{d}\mathbf{r}_1\, \phi_p^*(\mathbf{r}_1;\mathbf{R})\left(\frac{1}{2}\boldsymbol{\nabla}_1^2 + \sum_\nu^{N_\mathrm{n}} \frac{Z_\nu}{|\mathbf{r}_1 - \mathbf{R}_\nu|}\right)\phi_q(\mathbf{r}_1;\mathbf{R}), \tag{13}$$

$$\begin{aligned} v_{rs}^{pq}(\mathbf{R}) &= \delta_{\sigma_p\sigma_r}\delta_{\sigma_q\sigma_s}\tilde{v}_{rs}^{pq}(\mathbf{R}) \\ &= \delta_{\sigma_p\sigma_r}\delta_{\sigma_q\sigma_s}\iint \mathrm{d}\mathbf{r}_1\mathrm{d}\mathbf{r}_2\, \phi_p^*(\mathbf{r}_1;\mathbf{R})\phi_q^*(\mathbf{r}_2;\mathbf{R})\frac{1}{|\mathbf{r}_1 - \mathbf{r}_2|}\phi_r(\mathbf{r}_1;\mathbf{R})\phi_s(\mathbf{r}_2;\mathbf{R}), \end{aligned} \tag{14}$$

$$\mathbf{d}_{q,\nu}^p(\mathbf{R}) = \delta_{\sigma_p\sigma_q}\tilde{\mathbf{d}}_{q,\nu}^p(\mathbf{R}) = \delta_{\sigma_p\sigma_q}\int \mathrm{d}\mathbf{r}_1\, \phi_p^*(\mathbf{r}_1;\mathbf{R})\boldsymbol{\nabla}_\nu\phi_q(\mathbf{r}_1;\mathbf{R}), \tag{15}$$

$$\begin{aligned} g_q^p(\mathbf{R}) &= \delta_{\sigma_p\sigma_q}\tilde{g}_q^p(\mathbf{R}) \\ &= \delta_{\sigma_p\sigma_q}\sum_\nu \frac{1}{2M_\nu}\left(\int \mathrm{d}\mathbf{r}_1\, \phi_p^*(\mathbf{r}_1;\mathbf{R})\boldsymbol{\nabla}_\nu^\dagger\boldsymbol{\nabla}_\nu\phi_q(\mathbf{r}_1;\mathbf{R}) - \sum_r \mathbf{d}_{p,\nu}^{r\dagger}(\mathbf{R})\mathbf{d}_{q,\nu}^r(\mathbf{R})\right), \end{aligned} \tag{16}$$

where $\phi_p(\mathbf{r}_1;\mathbf{R})$ is spatial orbital p, σ_p is the corresponding electronic spin, δ is the Kronecker delta, and $\tilde{h}_q^p(\mathbf{R})$, $\tilde{v}_{rs}^{pq}(\mathbf{R})$, $\tilde{\mathbf{d}}_{q,\nu}^p(\mathbf{R})$ and $\tilde{g}_q^p(\mathbf{R})$ are spatial integrals. Without an external magnetic field, the orbitals can be real valued ($\phi_p^* = \phi_p$) without loss of generality.

The molecular Hamiltonian commutes with spin and electron number operators, and we can define a singlet excitation operator $\hat{E}_q^p = \hat{a}_{p\alpha}^\dagger\hat{a}_{q\alpha} + \hat{a}_{p\beta}^\dagger\hat{a}_{q\beta}$ for spins α and β. If $|\Phi\rangle$ includes only linear combinations of CSFs with a fixed spin and electron number, this yields the matrix form $\mathbb{E}_q^p = \langle\Phi|\hat{E}_q^p|\Phi\rangle^\mathsf{T}$. $\mathbb{H}_\mathrm{e}$ becomes

$$\mathbb{H}_\mathrm{e} = \sum_{pq}^{N_\mathrm{o}} \tilde{h}_q^p(\mathbf{R})\mathbb{E}_q^p + \frac{1}{2}\sum_{pqrs}^{N_\mathrm{o}} \tilde{v}_{rs}^{pq}(\mathbf{R})\left(\mathbb{E}_r^p\mathbb{E}_s^q - \mathbb{E}_s^p\delta_{qr}\right) + V_\mathrm{nn}(\mathbf{R}). \tag{17}$$

Similarly, $\mathbb{D}_\nu$ and $\mathbb{G}$ are expressed in terms of spatial integrals and $\mathbb{E}_q^p$. The above expression holds as long as $|\Phi\rangle$ spans the space of CSFs with a given electron number and spin, such that $|\Phi\rangle^\mathsf{T}\langle\Phi| = \mathbb{1}$.

2.3 Born-Oppenheimer and pre-Born-Oppenheimer frameworks

The Born-Oppenheimer (BO) approximation sets $\mathbb{D}_\nu$ and $\mathbb{G}$ to zero such that only $\mathbb{H}_\mathrm{e}$ and the bare nuclear kinetic energy remain, and the nuclear wavefunction evolves independently on each electronic state. The nonadiabatic coupling is required in order to describe internal conversion between electronic states. Methods beyond the BO approximation typically use eigenstates of $\hat{H}_\mathrm{e}$ as the many-body electronic basis ($\Phi_I(\mathbf{r};\mathbf{R})$), making $\mathbb{H}_\mathrm{e}$ diagonal. Expression of the molecular wavefunction in the form of Eq. 4 with eigenstates of $\hat{H}_\mathrm{e}$ is commonly known as the Born-Huang expansion[13]. Methods employing the Born-Huang expansion operate in a BO framework, since $\mathbb{D}_\nu$ and $\mathbb{G}$ act as corrections to the BO approximation.

Despite being theoretically exact, the choice of eigenstates of $\hat{H}_\mathrm{e}$ as the many-body electronic basis leads to several numerical problems for quantum molecular dynamics. The resulting Hamiltonian yields conical intersections, where BO potential energies have cusps, and derivative couplings $\mathbb{D}_\nu$ are localized and singular. Diagonalization of $\mathbb{H}_\mathrm{e}$ is also a cause of double-valued boundary conditions and the geometric phase effect[31]. An exact solution requires an infinite sum over states, whereas in practice the group BO approximation selects only a small set of BO electronic states and neglects $\mathbb{G}$ and $\mathbb{D}_\nu^\dagger\mathbb{D}_\nu$ terms outside of the set. $\mathbb{G}$ and $\mathbb{D}_\nu^\dagger\mathbb{D}_\nu$ are often entirely neglected as a first-order approximation of the nonadiabatic coupling since their magnitudes are low whereas they have a high computational cost[13].

View Article Online
DOI: 10.1039/D6FD00096G

Choosing a separate many-body electronic basis without special treatment of $\hat{H}_\mathrm{e}$ results in a pre-BO ansatz, since the BO states are not involved in the simulation. An ideal basis would also remove discontinuities in the Hamiltonian by ensuring that it varies smoothly with nuclear coordinates[38]. To simplify the choice of many-body basis, we consider a basis of individual CSFs rather than their linear combinations. In Section 2.4 we derive the equations for an active space approximation to reduce the number of CSFs and thus the computational cost. By propagating the orbitals in such a way that each orbital is a smooth function of $\mathbf{R}$, we obtain smooth surfaces without cusps or singularities because all of the spatial dependence is given by one- and two-electron spatial integrals. Details of the orbital propagation are provided in Section 2.5.

2.4 Active space approximation

The number of CSFs has a combinatorial dependence on the number of orbitals, the number of electrons, and the electronic spin. In practical cases, the spin is small (often zero) and the number of orbitals is proportional to the number of electrons. This leads to a rapid growth in the many-electron basis that underpins one of the primary computational challenges of electronic structure theory. Using the full set of CSFs is equivalent to full configuration interaction (FCI), which provides the exact eigenstates of the BO electronic Hamiltonian for the chosen orbital basis set.

To reduce the number of CSFs, we can designate a subset of orbitals as active orbitals (labeled p, q, r and s) and consider every excitation within the subset. The remaining orbitals are either doubly occupied (labeled a and b) or virtual (labeled j and k). The active space approximation removes all excitations between orbital spaces ($\langle \hat{E}^p_a \rangle = \langle \hat{E}^j_a \rangle = \langle \hat{E}^j_p \rangle = 0$), and fixes $\langle \hat{E}^b_a \rangle = 2\delta_{ab}$ and $\langle \hat{E}^k_j \rangle = 0$. As a result, the molecular Hamiltonian is approximated by

$$\mathbb{H}^\mathrm{act}_\mathrm{mol} = \sum_\nu \frac{1}{2M_\nu} |\boldsymbol{\nabla}_\nu + \mathbb{D}^\mathrm{act}_\nu|^2 + \mathbb{V}^\mathrm{act}, \tag{18}$$

where $\mathbb{D}^\mathrm{act}_\nu$ takes the same form as $\mathbb{D}_\nu$ but only includes active orbitals p and q. The potential energy $\mathbb{V}^\mathrm{act}$ is given by

$$\mathbb{V}^\mathrm{act} = \sum_{pq}^{N_\mathrm{o}} \tilde{k}^p_q(\mathbf{R}) \mathbb{E}^p_q + \frac{1}{2} \sum_{pqrs}^{N_\mathrm{o}} \tilde{v}^{pq}_{rs}(\mathbf{R}) \mathbb{E}^p_r \mathbb{E}^q_s + V_\mathrm{cons}(\mathbf{R}), \tag{19}$$

where the one-electron coefficients and the constant term are given by

$$\begin{aligned} \tilde{k}^p_q(\mathbf{R}) = \tilde{h}^p_q(\mathbf{R}) + \sum_a \left(2\tilde{v}^{pa}_{qa}(\mathbf{R}) - \tilde{v}^{ap}_{qa}(\mathbf{R}) - \sum_\nu \frac{1}{2M_\nu} \tilde{\mathbf{d}}^{a\dagger}_{p,\nu}(\mathbf{R}) \tilde{\mathbf{d}}^a_{q,\nu}(\mathbf{R}) \right) \\ + \frac{1}{2} \left(\tilde{g}^p_q(\mathbf{R}) - \sum_r \tilde{v}^{pr}_{rq}(\mathbf{R}) \right), \end{aligned} \tag{20}$$

$$V_\mathrm{cons}(\mathbf{R}) = V_\mathrm{nn}(\mathbf{R}) + \sum_a \left(2\tilde{h}^a_a(\mathbf{R}) + \tilde{g}^a_a(\mathbf{R}) + \sum_b \left(2\tilde{v}^{ab}_{ab}(\mathbf{R}) - \tilde{v}^{ab}_{ba}(\mathbf{R}) \right) \right), \tag{21}$$

where $\tilde{g}^p_q(\mathbf{R})$ is defined as in Eq. 12 with a sum over only active orbitals r, and $\tilde{g}^a_a(\mathbf{R})$ involves only doubly occupied orbitals b in place of r. The extra terms $\tilde{\mathbf{d}}^{a\dagger}_{p,\nu}(\mathbf{R}) \tilde{\mathbf{d}}^a_{q,\nu}(\mathbf{R})$ arise from the difference $\mathbb{D}^\dagger_\nu \mathbb{D}_\nu - \mathbb{D}^{\mathrm{act}\dagger}_\nu \mathbb{D}^\mathrm{act}_\nu$.

If all terms containing $\tilde{g}^p_q$ and $\tilde{\mathbf{d}}^p_{q,\nu}$ and equivalent terms for doubly occupied orbitals are ignored, the remaining Hamiltonian is $\mathbb{H}^\mathrm{act}_\mathrm{e}$. Specifically, this is the Hamiltonian for complete active space configuration interaction (CASCI). Employing the active space approximation with the wavefunction ansatz described above is thus theoretically equivalent to simulations with CASCI potential energy surfaces and couplings.

View Article Online
DOI: 10.1039/D6FD00096G

2.5 Orbital propagation

In order to ensure that the elements of the Hamiltonian vary slowly and continuously as a function of nuclear position, we adopt a scheme to propagate orbitals continuously between nuclear positions. The molecular orbitals (MOs) are expanded in an electronic basis set

$$|\Phi(\mathbf{R})\rangle^{\mathsf{T}} = |\eta(\mathbf{R})\rangle^{\mathsf{T}}\, \mathbb{c}(\mathbf{R}), \tag{22}$$

where $|\Phi(\mathbf{R})\rangle$ is a vector of MOs with elements $|\phi_p(\mathbf{R})\rangle$, $|\eta(\mathbf{R})\rangle$ is a vector of basis functions, and $\mathbb{c}(\mathbf{R})$ is a matrix of expansion coefficients. In general, the basis set may be non-orthogonal and we can define an overlap matrix $\mathbb{S}(\mathbf{R}) = \langle \eta(\mathbf{R})|\eta(\mathbf{R})\rangle_{\mathbf{r}}^{\mathsf{T}}$. Electronic basis sets can be chosen to be independent of nuclear positions, such as plane wave bases, in which case much of the following derivation does not apply. Going forward, we assume an atom-centered orbital basis set with explicit dependence of the basis on the nuclear positions.

We use the electronic overlap between adjacent nuclear positions $\mathbf{R}' = \mathbf{R} - \delta\mathbf{R}$ and $\mathbf{R}$ to propagate the molecular orbital coefficients from $\mathbb{c}(\mathbf{R}')$ to $\mathbb{c}(\mathbf{R})$. We define a MO overlap matrix

$$\mathbb{O}(\mathbf{R},\mathbf{R}') = \mathbb{c}_{\mathrm{loc}}^{\dagger}(\mathbf{R})\mathbb{S}(\mathbf{R})\mathbb{c}(\mathbf{R}'), \tag{23}$$

where $\mathbb{c}_{\mathrm{loc}}(\mathbf{R}')$ are MO coefficients based on only local information at $\mathbf{R}$. We then choose the propagation of MO coefficients given by

$$\mathbb{c}(\mathbf{R}) = \mathbb{c}_{\mathrm{loc}}(\mathbf{R})\mathbb{O}(\mathbf{R},\mathbf{R}')(\mathbb{O}^{\dagger}(\mathbf{R},\mathbf{R}')\mathbb{O}(\mathbf{R},\mathbf{R}'))^{-1/2}. \tag{24}$$

Without loss of generality, the dependence on $\mathbb{c}_{\mathrm{loc}}(\mathbf{R})$ can be removed because $\mathbb{c}_{\mathrm{loc}}(\mathbf{R})\mathbb{c}_{\mathrm{loc}}^{\dagger}(\mathbf{R}) = \mathbb{S}^{-1}(\mathbf{R})$. This yields the transformation $\mathbb{c}(\mathbf{R}) = \mathbb{c}(\mathbf{R}')\mathbb{W}^{-1/2}(\mathbf{R},\mathbf{R}')$, where $\mathbb{W}(\mathbf{R},\mathbf{R}') = \mathbb{c}^{\dagger}(\mathbf{R}')\mathbb{S}(\mathbf{R})\mathbb{c}(\mathbf{R}')$, which approaches $\mathbb{1}$ as $\mathbf{R}$ approaches $\mathbf{R}'$.

When using an active space, $\mathbb{W}(\mathbf{R},\mathbf{R}')$ gradually mixes molecular orbitals between different spaces. To mitigate this effect, we divide $\mathbb{c}$ into doubly occupied, active, and virtual spaces: $\mathbb{c}_{\mathrm{docc}}$, $\mathbb{c}_{\mathrm{act}}$ and $\mathbb{c}_{\mathrm{virt}}$. Simply replacing $\mathbb{c}$ with the coefficients in each space leads to non-orthogonal MOs. We use Gram-Schmidt orthogonalization with a projector given by $\mathbb{P}_Q = \mathbb{O}_Q(\mathbb{O}_Q^{\dagger}\mathbb{O}_Q)^{-1}\mathbb{O}_Q^{\dagger}$ where Q is the space. We then project out doubly occupied and active spaces: $\mathbb{O}_{\mathrm{act}} \to (\mathbb{1} - \mathbb{P}_{\mathrm{docc}})\mathbb{O}_{\mathrm{act}}$ and $\mathbb{O}_{\mathrm{virt}} \to (\mathbb{1} - \mathbb{P}_{\mathrm{docc}} - \mathbb{P}_{\mathrm{act}})\mathbb{O}_{\mathrm{virt}}$. This yields

$$\mathbb{c}_Q(\mathbf{R}) = \mathbb{S}^{-1}(\mathbf{R})\mathbb{S}_Q(\mathbf{R},\mathbf{R}')\mathbb{c}_Q(\mathbf{R}')\mathbb{W}_Q^{-1/2}(\mathbf{R},\mathbf{R}'), \tag{25}$$

where $\mathbb{W}_Q(\mathbf{R},\mathbf{R}') = \mathbb{c}_Q^{\dagger}(\mathbf{R}')\mathbb{S}_Q(\mathbf{R},\mathbf{R}')\mathbb{c}_Q(\mathbf{R}')$, and the effective overlap matrix is given for each space by

$$\mathbb{S}_{\mathrm{docc}}(\mathbf{R},\mathbf{R}') = \mathbb{S}(\mathbf{R}), \tag{26}$$

$$\mathbb{S}_{\mathrm{act}}(\mathbf{R},\mathbf{R}') = \mathbb{S}(\mathbf{R}) - \mathbb{c}_{\mathrm{docc}}(\mathbf{R}')\left(\mathbb{c}_{\mathrm{docc}}^{\dagger}(\mathbf{R}')\mathbb{S}(\mathbf{R})\mathbb{c}_{\mathrm{docc}}(\mathbf{R}')\right)^{-1}\mathbb{c}_{\mathrm{docc}}^{\dagger}(\mathbf{R}'), \tag{27}$$

$$\begin{aligned}\mathbb{S}_{\mathrm{virt}}(\mathbf{R},\mathbf{R}') = {}& \mathbb{S}(\mathbf{R}) - \mathbb{c}_{\mathrm{docc}}(\mathbf{R}')\left(\mathbb{c}_{\mathrm{docc}}^{\dagger}(\mathbf{R}')\mathbb{S}(\mathbf{R})\mathbb{c}_{\mathrm{docc}}(\mathbf{R}')\right)^{-1}\mathbb{c}_{\mathrm{docc}}^{\dagger}(\mathbf{R}') \\ & - \mathbb{c}_{\mathrm{act}}(\mathbf{R}')\left(\mathbb{c}_{\mathrm{act}}^{\dagger}(\mathbf{R}')\mathbb{S}(\mathbf{R})\mathbb{c}_{\mathrm{act}}(\mathbf{R}')\right)^{-1}\mathbb{c}_{\mathrm{act}}^{\dagger}(\mathbf{R}').\end{aligned} \tag{28}$$

$\mathbb{P}_Q$ and $\mathbb{S}_Q$ are related by $\mathbb{P}_Q = \mathbb{c}_{\mathrm{loc}}^{\dagger}\mathbb{S}_Q\mathbb{c}_{\mathrm{loc}}$.

The calculation of $\tilde{\mathbf{d}}_{q,\nu}^{p}(\mathbf{R})$ and $\tilde{g}_q^p(\mathbf{R})$ require gradients of the MO coefficients, given by $\boldsymbol{\nabla}_\nu\mathbb{c}(\mathbf{R}) = \mathbb{c}(\mathbf{R}')\boldsymbol{\nabla}_\nu\mathbb{W}^{-1/2}(\mathbf{R},\mathbf{R}')$. The gradient of the transformation $\mathbb{W}^{-1/2}(\mathbf{R},\mathbf{R}')$ is evaluated by solving a Sylvester equation

$$\mathbb{W}^{-1/2}\left(\boldsymbol{\nabla}_\nu\mathbb{W}^{-1/2}\right) + \left(\boldsymbol{\nabla}_\nu\mathbb{W}^{-1/2}\right)\mathbb{W}^{-1/2} = -\mathbb{W}^{-1}\left(\boldsymbol{\nabla}_\nu\mathbb{W}\right)\mathbb{W}^{-1}, \tag{29}$$

View Article Online
DOI: 10.1039/D6FD00096G

where the dependence on $\mathbf{R}$ and $\mathbf{R}'$ has been dropped for convenience. The gradient on the right hand side then simplifies to $\boldsymbol{\nabla}_\nu \mathbb{W}(\mathbf{R},\mathbf{R}') = \mathbb{c}^\dagger(\mathbf{R}')(\boldsymbol{\nabla}_\nu \mathbb{S}(\mathbf{R}))\mathbb{c}(\mathbf{R}')$, which can be readily computed with integral packages. The active space approximation also only requires the gradient $\boldsymbol{\nabla}_\nu \mathbb{S}(\mathbf{R})$ since all other elements depend on $\mathbf{R}'$.

2.6 Mixed quantum-classical dynamics

The simulation of photochemical dynamics with the Hamiltonian described in the previous sections requires pre-calculation of the orbitals and the Hamiltonian for regions of $\mathbf{R}$ that are energetically accessible. Instead, we adopt a mixed quantum-classical (MQC) approach, which simplifies the nuclear wavefunction to an ensemble of classical trajectories. By using an MQC approach, the Hamiltonian can be calculated on-the-fly as the trajectories evolve. We adopt average-potential based MQC approaches such as Ehrenfest dynamics because the electronic Hamiltonian is not diagonal in the CSF basis. The only additional step required is sampling of initial conditions to reproduce the nuclear probability density.

One can derive exact mixed quantum-classical equations from the exact factorization formalism, where a molecular wavefunction is expressed as a single product of time-dependent nuclear and electronic wave functions

$$|\Psi_{\mathrm{mol}}(\mathbf{R},t)\rangle = \chi(\mathbf{R},t)\,|\Phi_{\mathbf{R}}(t)\rangle\,. \tag{30}$$

The electronic wavefunction satisfies the partial normalization condition at all $\mathbf{R}$ and t: $\langle\Phi_{\mathbf{R}}(t)|\Phi_{\mathbf{R}}(t)\rangle_{\mathbf{r}} = 1$. Consequently, the molecular dynamics is described by a set of equations of motion for nuclear and electronic wavefunctions coupled via an electron-nuclear correlation (ENC) operator and time-dependent vector and scalar potentials. A detailed discussion including derivation and analysis of equations for exact factorization is available in refs. 49 and 50.

The time evolution of the many-body electronic basis coefficients and the nuclear force are given as $\dot{C}_J = \dot{C}_J^{\mathrm{Eh}} + \dot{C}_J^{\mathrm{ENC}}$ and $\mathbf{F}_\nu = \mathbf{F}_\nu^{\mathrm{Eh}} + \mathbf{F}_\nu^{\mathrm{ENC}}$, respectively, where the ENC terms appears in addition to the Ehrenfest (Eh) terms:

$$\dot{C}_J^{\mathrm{Eh}} = -i\sum_K H_{e,JK}C_K - \sum_K\sum_\nu \frac{1}{M_\nu}\mathbf{P}_\nu^{\mathsf{T}}\mathbf{D}_{\nu,JK}C_K, \tag{31}$$

$$\dot{C}_J^{\mathrm{ENC}} = -\sum_K\left\{\sum_\nu \frac{1}{2M_\nu}\left(\boldsymbol{\mathcal{G}}_{\nu,JK} - \boldsymbol{\mathcal{P}}_\nu + \boldsymbol{\nabla}_\nu\right)^{\mathsf{T}}\boldsymbol{\mathcal{F}}_{\nu,JK}\right\}|C_K|^2 C_J, \tag{32}$$

$$\mathbf{F}_\nu^{\mathrm{Eh}} = -\sum_{JK} C_J^*(\boldsymbol{\nabla}_\nu H_{e,JK})C_K - \sum_{JK} C_J^* C_K \sum_L \left(\mathbf{D}_{\nu,LJ}^* H_{e,LK} + H_{e,JL}\mathbf{D}_{\nu,LK}\right), \tag{33}$$

$$\mathbf{F}_\nu^{\mathrm{ENC}} = -\sum_{JK}\boldsymbol{\mathcal{F}}_{\nu,JK}\left\{\sum_\mu \frac{1}{2M_\mu}\left(\boldsymbol{\mathcal{G}}_{\mu,JK} - \boldsymbol{\mathcal{P}}_\mu + \boldsymbol{\nabla}_\mu\right)^{\mathsf{T}}\boldsymbol{\mathcal{F}}_{\mu,JK}\right\}|C_J|^2|C_K|^2, \tag{34}$$

where $\mathbf{P}_\nu$ is the nuclear momentum, $C_J = |C_J|e^{iS_J}$ is the expansion coefficient for the electronic state, $|\Phi_{\mathbf{R}}(t)\rangle = \sum_J C_J|\Phi_J\rangle$, $\boldsymbol{\mathcal{F}}_{\nu,JK} = \boldsymbol{\nabla}_\nu S_J - \boldsymbol{\nabla}_\nu S_K$ is the difference of the phase term[52], $\boldsymbol{\mathcal{P}}_\nu = (\boldsymbol{\nabla}_\nu|\chi|^2)/|\chi|^2$ is the total quantum momentum, and $\boldsymbol{\mathcal{G}}_{\nu,JK} = (\boldsymbol{\nabla}_\nu|\chi_J|^2)/|\chi_J|^2 + (\boldsymbol{\nabla}_\nu|\chi_K|^2)/|\chi_K|^2$ is the projected quantum momentum. For our MQC equations, we adopt the gauge condition that the time-dependent scalar potential vanishes[58].

The calculation of total and projected quantum momentum terms are straightforward from the definition of the total and projected nuclear densities. If we expand the electronic state of the Eq. 30 $|\Phi_{\mathbf{R}}(t)\rangle = \sum_J C_J|\Phi_J\rangle$ and compare it with Eq. 4, we obtain $\chi_J(\mathbf{R},t) = C_J(\mathbf{R},t)\chi(\mathbf{R},t)$ and thus $|\chi|^2 = \sum_J|\chi_J|^2$, where the nuclear densities can be constructed from the spatial distribution of trajectories and their populations. We define the BO projected nuclear density for each state as a multi-dimensional

View Article Online
DOI: 10.1039/D6FD00096G

Gaussian function based on the nuclear configurations and BO populations of trajectories[53],

$$|\chi_J(\mathbf{R},t)|^2 \equiv \frac{\langle |C_J|^2 \rangle(t)}{\mathcal{N}_J(t)} \prod_\nu \exp\left(-\frac{|\mathbf{R}_\nu - \mathbf{R}_{\nu,J}(t)|^2}{2\sigma_{\nu,J}(t)^2}\right), \tag{35}$$

where $\mathcal{N}_i$ is the normalization factor. The center and variance of the Gaussian for each state are then defined as

$$\mathbf{R}_{\nu,J}(t) = \frac{\sum_k^{N_{\text{traj}}} |C_J^{(k)}(t)|^2 \mathbf{R}_\nu^{(k)}(t)}{\sum_k^{N_{\text{traj}}} |C_J^{(k)}(t)|^2}, \tag{36}$$

$$\sigma_{\nu,J}^2(t) \equiv \frac{\sum_k^{N_{\text{traj}}} |C_J^{(k)}(t)|^2 |\mathbf{R}_\nu^{(k)}(t) - \mathbf{R}_{\nu,J}(t)|^2}{\sum_k^{N_{\text{traj}}} |C_J^{(k)}(t)|^2}, \tag{37}$$

where N_{traj} denotes the number of trajectories and k is the trajectory index. As a result, we find

$$\mathcal{G}_{\nu,JK}(\mathbf{R}) = -\left[\left(\frac{1}{\sigma_{\nu,J}^2} + \frac{1}{\sigma_{\nu,K}^2}\right)\mathbf{R}_\nu - \left(\frac{\mathbf{R}_{\nu,J}}{\sigma_{\nu,J}^2} + \frac{\mathbf{R}_{\nu,K}}{\sigma_{\nu,K}^2}\right)\right], \tag{38}$$

$$\mathcal{P}_\nu = -\left[\sum_J \left(\frac{|C_J|^2}{\sigma_{\nu,J}^2}\right)\mathbf{R}_\nu - \sum_J \left(\frac{|C_J|^2 \mathbf{R}_{\nu,J}}{\sigma_{\nu,J}^2}\right)\right]. \tag{39}$$

The divergence of the phase term $\boldsymbol{\nabla}_\nu^{\mathsf{T}} \boldsymbol{\mathcal{F}}_{\nu,JK}$, which is crucial for the correct net population transfer conservation, is usually approximated as a uniform function $\Delta_{\nu,jk}$ to avoid the second-order derivative term calculation[58],

$$\Delta_{\nu,JK} = -\frac{\sum_k^{N_{\text{traj}}} \left(\left\{\left(\boldsymbol{\mathcal{G}}_{\nu,JK} - \boldsymbol{\mathcal{P}}_\nu\right)^{\mathsf{T}} \boldsymbol{\mathcal{F}}_{\nu,JK}\right\} |C_J|^2 |C_K|^2\right)^{(k)}}{\sum_k^{N_{\text{traj}}} \left(|C_J|^2 |C_K|^2\right)^{(k)}}. \tag{40}$$

The definition of the phase term $\boldsymbol{\mathcal{F}}_{\nu,JK}$ in the CSF basis becomes ambiguous compared its counterpart in the BO basis. In the BO basis the phase term $\boldsymbol{\nabla}_\nu S_J$ can be approximated as a state-wise BO momentum[56,58] or a BO force integration[52], both exploiting the conceptually well-defined potential energy surface of each BO state. However, in the CSF basis, such approximations are not directly applicable due to the off-diagonal terms of the electronic Hamiltonian. Nonetheless, we can use an analogous definition of the effective potential energy of each CSF state deduced similarly from Eq. 31:

$$E_J^{\text{CSF}} \equiv \frac{\sum_K \Re(C_J^* H_{e,JK} C_K)}{|C_J|^2} \tag{41}$$

such that

$$E_{\text{pot}} = \sum_J |C_J|^2 E_J^{\text{CSF}}. \tag{42}$$

We then approximate the phase term to the state-wise CSF momentum parallel to the true momentum as

$$\boldsymbol{\nabla}_\nu S_J \approx \mathbf{P}_{\nu,J} \equiv \mathbf{P}_\nu \sqrt{\max\left(0, \frac{E_{\text{tot}} - E_J^{\text{CSF}}}{E_{\text{kin}}}\right)} \tag{43}$$

We neglect the recently derived phase correction term[58] since it is very sensitive to the accuracy of the phase terms, and it would have a more significant effect with the CSF basis.

View Article Online
DOI: 10.1039/D6FD00096G

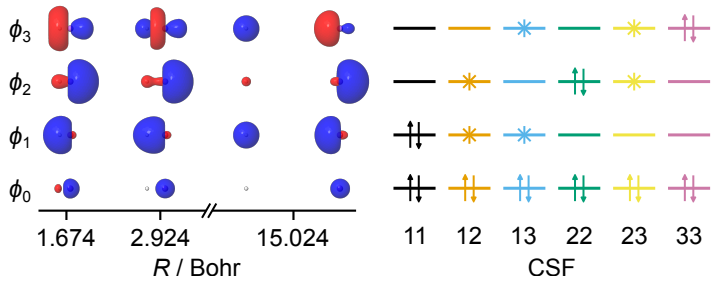

Figure 1 Molecular orbitals and CSFs of LiH. The set of orbitals (ϕ_0–ϕ_3) are propagated so that they change smoothly as a function of bond length, R. The lowest energy CSFs all have ϕ_0 doubly occupied, so they are labeled by the remaining MO occupations.

3 Results and Discussion

3.1 Lithium hydride

As a proof-of-concept demonstration, we test the MQC dynamics in the full configuration interaction CSF basis with orbital propagation on the excited state dynamics of lithium hydride (LiH) with a minimal STO-3G basis. We only consider Σ^+ states, and the linear symmetry allows us to reduce the basis set to two s and one p_z atomic orbitals on the Li atom and one s atomic orbital on the H atom, where z is the internuclear axis. This results in a total of 20 CSFs for neutral LiH. To provide a comparison to the exact solution, we first obtained the Hartree-Fock (HF) MOs at the optimized FCI equilibrium geometry ($R = 2.924$ Bohr). We then propagated the orbitals (Section 2.5) with a sampling distance of $\Delta R = 0.05$. We used the calculated Hamiltonian to perform quantum wavepacket dynamics (Eqs. 8 and 9). We used the PySCF package[59] for electronic structure calculations including electronic integrals, CSF matrix elements, and FCI, and we used geomeTRIC backend of PySCF for geometry optimization[60].

The MOs and low energy CSFs used in the simulation are shown in Fig. 1. The MOs are ordered by their HF orbital energies at the equilibrium geometry. ϕ_0 is predominantly the Li $1s$ core orbital, ϕ_1 is the bonding orbital, and ϕ_2 and ϕ_3 are anti-bonding orbitals. The orbital propagation results in delocalization across Li and H at long bond lengths while retaining the overall characteristics of the orbitals at the equilibrium geometry. The six lowest energy CSFs each have ϕ_0 doubly occupied, so they are labeled by the occupation of the remaining orbitals.

In Fig. 2, we show the matrix elements of the electronic Hamiltonian, $\mathbb{H}_e$. The energies of CSFs with partially occupied ϕ_0 are over 1.5 E_h higher in energy and are not shown. The diagonal matrix elements of CSFs 11, 12, 23 and 33 each approach the same asymptotic limit with the covalent character of LiH. CSFs 22 and 13, on the other hand, tend to an ionic configuration with the electron density localized on one atom. Off diagonal elements (Fig. 2b) of $\mathbb{H}_e$ reach constant values as R increases. The largest values are caused by the delocalization of the orbitals. In particular, ϕ_1 and ϕ_3 are the sum and difference of the H $1s$ orbital and a Li $2s$-$2p$ hybrid orbital and the large coupling of CSFs 11 and 33 as well as 12 and 23 suggest that localized orbitals would lower their magnitude.

The elements of the derivative coupling $\mathbb{D}$ (Fig. 2c) have magnitudes comparable to off diagonal elements of $\mathbb{H}_e$, but they have units of momentum. Their effect on the dynamics is negligible since they would require a nuclear kinetic energy of $\sim 800\ E_\mathrm{h}$ to yield energies proportional to off-diagonal elements of $\mathbb{H}_e$. Calculation of $\mathbb{G}$ was beyond the scope of the current work, but the magnitude of its values are

View Article Online
DOI: 10.1039/D6FD00096G

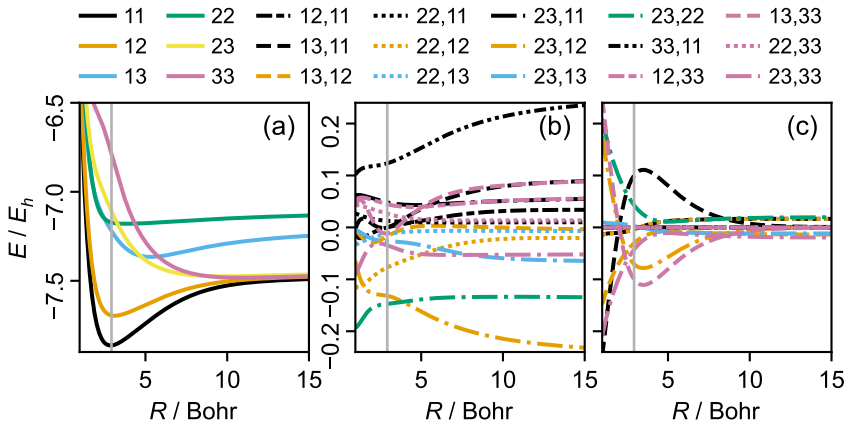

Figure 2 Elements of the LiH Hamiltonian in the CSF basis. The equilibrium geometry is shown by a grey line. (a) Diagonal matrix elements of the electronic Hamiltonian, $H_{e,II}$. (b) Off-diagonal matrix elements of the electronic Hamiltonian, $H_{e,IJ}$. (c) Matrix elements of the derivative coupling, D_{IJ}. Units of D_{IJ} are a.u.

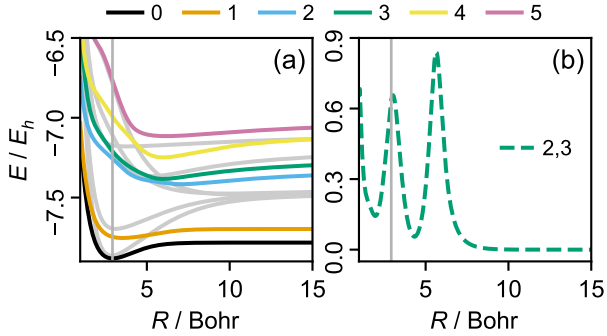

Figure 3 Elements of the LiH Hamiltonian in the BO basis. (a) BO potential energies from FCI. Diagonal elements of the electronic Hamiltonian in the CSF basis are show in grey. (b) Nonadiabatic couplings between BO states 2 and 3.

likely on the order $\mathbb{D}^2/M$ with a reduced mass M, and are thus even smaller than the derivative couplings.

To provide a comparison to the BO basis, we provide the FCI potential energies in Fig. 3a equivalent to the eigenvalues of $\mathbb{H}_e$. The BO electronic states separate into three pairs as the bond length increases, with many avoided crossings near the equilibrium geometry. In Fig. 3b we focus on the nonadiabatic couplings between BO states 2 and 3, with characteristic peaks centered at the avoided crossings. The strong coupling between BO states and their energetic separation from the other states makes them a reasonable choice for wavepacket dynamics simulations. Fig. 4 shows the square overlaps of each CSF for the four lowest BO states, given by $|\langle\Phi_I^{\mathrm{BO}}|\Phi_J^{\mathrm{CSF}}\rangle|^2$. BO states 0 and 1 are dominated by single CSFs (11 and 12, respectively) at equilibrium, but develop a mixed character with longer bond lengths and delocalized orbitals. In contrast, BO states 2 and 3 have a mixed character at equilibrium and at longer bond lengths. The change in CSFs highlights the complex interplay of electronic characters in the BO basis for changing nuclear coordinates.

For the quantum wavepacket dynamics, we prepared a Gaussian nuclear wavefunc-

View Article Online
DOI: 10.1039/D6FD00096G

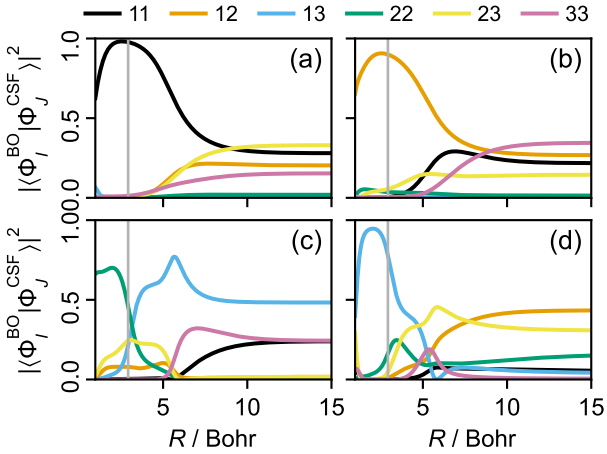

Figure 4 Square overlaps of CSFs for BO states as a function of LiH bond length. (a) $I = 0$. (b) $I = 1$. (c) $I = 2$. (d) $I = 3$.

tion on $|\Phi_2^{\mathrm{BO}}\rangle$ centered at the equilibrium geometry $R_0 = 2.924$ Bohr. We used a width $\sigma = 1/\sqrt{2M\omega}$ where $\omega = 0.00766$ a.u. is the harmonic frequency obtained from FCI calculation and $M = 1604.38$ a.u. is the reduced mass. The initial state was given by

$$|\Psi(R,0)\rangle = \chi(R,0)\,|\Phi_2^{\mathrm{BO}}(R)\rangle = (2\pi\sigma^2)^{-1/4}\exp\left(-\frac{(R-R_0)^2}{4\sigma^2}\right)|\Phi_2^{\mathrm{BO}}(R)\rangle\,. \qquad (44)$$

We used a sinc discrete variable representation for the nuclear grid, $R \in [0.974, 25.024]$ Bohr with $\Delta R = 0.05$ Bohr, and a time-interval of $\Delta t = 2.0$ a.u. The wavefunction was evolved in the CSF basis for direct comparison to MQC results.

In Fig. 5, we show the populations $\langle|C_I|^2\rangle$ and coherences $\langle|C_I|^2|C_J|^2\rangle$ of the quantum dynamics of LiH in the BO and CSF bases. The populations in the BO basis (Fig. 5a) show the expected population transfer between BO states 2 and 3 at $t = 300$ a.u., after which the populations stabilize. The time evolution leads to dissociation of the LiH bond, leading to a gradual mixing of CSFs shown in Fig. 5b. The oscillatory behaviour of CSF populations occurs due to the constant off-diagonal values of $\mathbb{H}_e$ at long bond lengths.

The BO coherence (Fig. 5c) between states 2 and 3 shows a sharp rise during population transfer, followed by a gradual decrease as the wavepackets on the two BO states separate due to their different potential and kinetic energies. The CSF coherences (Fig. 5d) show more complex behaviour that reflects the CSF composition of the populated BO states as well as the time evolution of CSF populations. Interestingly, the CSF coherences also gradually approach zero with increasing time despite the sustained oscillations of CSF populations. The two largest values of coherence at $t = 1000$ a.u. are between CSFs 11 and 13, and 33 and 13, which are the populated CSFs of BO state 2 at long bond lengths.

We performed MQC dynamics simulations by sampling 100 initial positions and momenta from the Wigner distribution of the initial state (Eq. 44)[61,62]. For each trajectory we used the FCI state at the sampled geometry as the initial electronic state. The MOs were propagated along the trajectory with timesteps of $\Delta t = 2$ a.u., and the Hamiltonian was calculated in the CSF basis at each timestep.

The Eherenfest dynamics result (Fig. 6) shows excellent agreement for population dynamics in both the BO and CSF bases. However, the BO coherences (Fig. 6c)

View Article Online
DOI: 10.1039/D6FD00096G

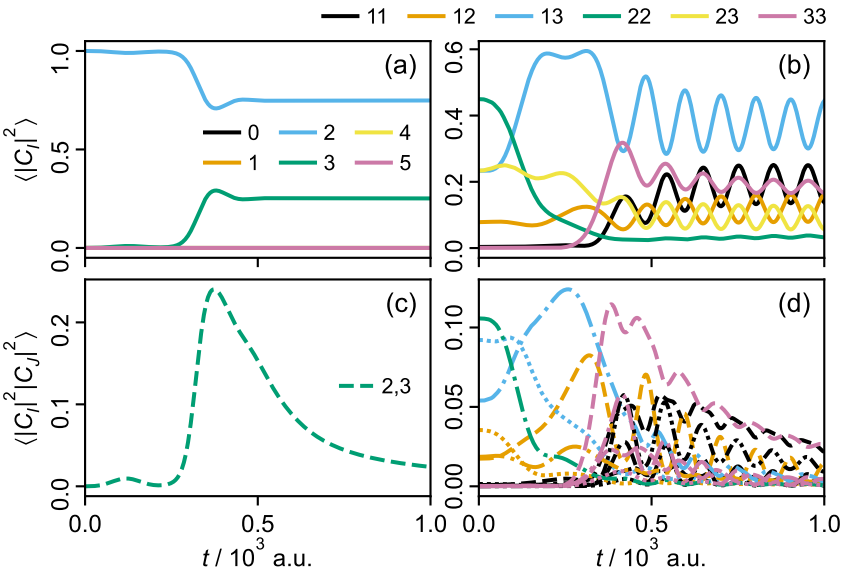

Figure 5 Electronic dynamics obtained from exact quantum wave packet dynamics simulation. (a) Populations of BO states. (b) Populations of CSFs. (c) Coherences between BO states 2 and 3. (d) Coherences between CSFs. Refer to Fig. 2 for line labels.

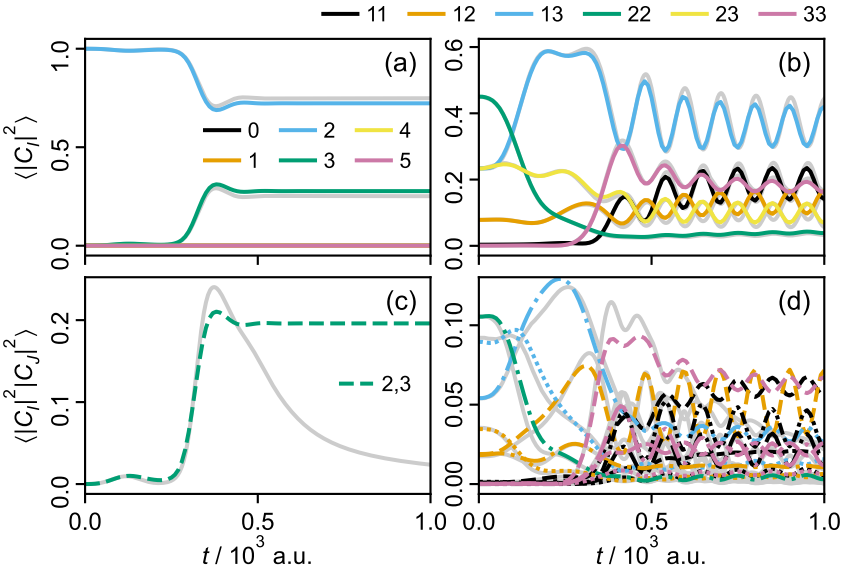

Figure 6 Electronic dynamics obtained from Ehrenfest dynamics simulation. Exact results are shown as grey lines for comparison. (a) Populations of BO states. (b) Populations of CSFs. (c) Coherences between BO states 2 and 3. (d) Coherences between CSFs. Refer to Fig. 2 for line labels.

View Article Online
DOI: 10.1039/D6FD00096G

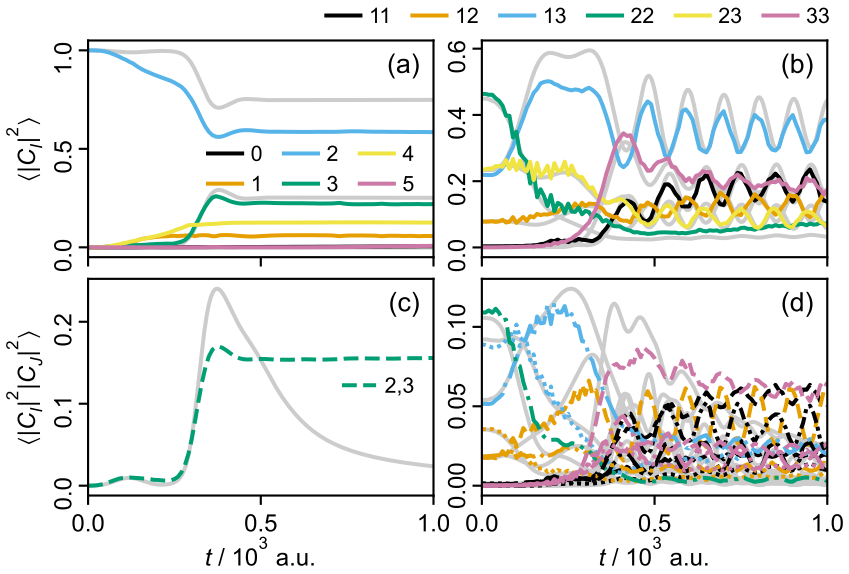

Figure 7 Electronic dynamics obtained from coupled trajectory dynamics simulation. Exact results are shown as grey lines for comparison. (a) Populations of BO states. (b) Populations of CSFs. (c) Coherences between BO states 2 and 3. (d) Coherences between CSFs. Refer to Fig. 2 for line labels.

show the over-coherence effect after the population transfer. The Ehrenfest dynamics evolve on an average potential energy surface, meaning the nuclear wavepacket cannot decohere without reaching another strong coupling region on the potential energy surface. Consequently, in the CSF basis the coherences oscillate around constant values that reflect the two populated BO states. Whereas the only disagreement with the exact result stems from slight differences in the nuclear wavepackets, the over-coherence has the potential to alter the electronic dynamics as well in larger molecules with more degrees of freedom.

In an attempt to correct for the over-coherence of the Ehrenfest dynamics, we performed coupled-trajectory (CT) dynamics simulations. The results in Fig. 7 show that the ENC effect is immediately non-zero in the CSF basis as the initial state is a BO state and CSF states are coherent at the beginning of the dynamics. Ideally, a correct reproduction of the ENC effect should initially have an average net effect of zero considering the initial accuracy of the Ehrenfest dynamics. However, the CT results show inaccurate electronic dynamics even before the initial population transfer seen in the exact result. Around $t = 100$ a.u., the CT trajectories undergo partial population transfer to BO states 1 and 4. In the CSF basis, this population change manifests as suppressed population of CSF 13 and increased population of several other CSFs, particularly CSF 22. Furthermore, the BO and CSF coherences (Fig. 7c and d) persist similar to the Eh results with a lower magnitude, indicating persistent over-coherence.

Fig. 8 shows a comparison of nuclear densities for two representative timesteps, $t = 350$ a.u. and 840 a.u. At the earlier time, the nuclear wavepacket remains localized as the electronic population transfer proceeds between BO states 2 and 3. The Ehrenfest and CT trajectories have a wider distribution than the exact nuclear wavepacket, and the CT results in particular has trajectories around $R = 3$ and 9 Bohr. This disagreement is a direct result of the incorrect ENC force leading to

View Article Online
DOI: 10.1039/D6FD00096G

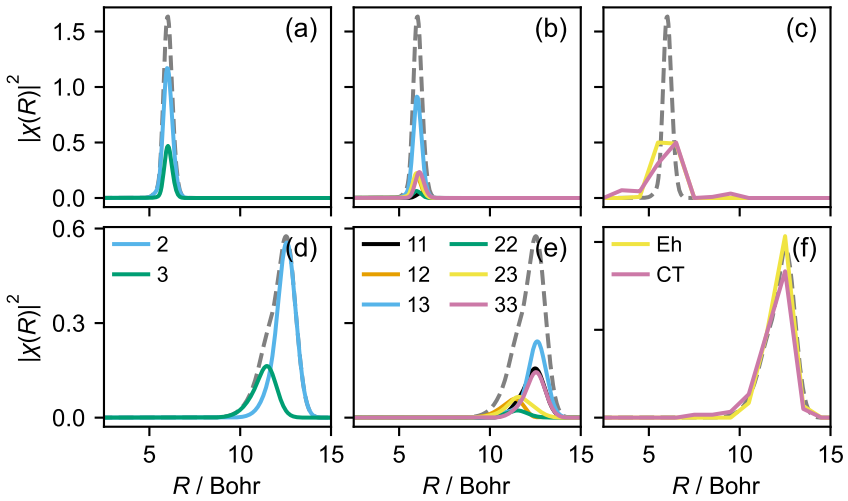

Figure 8 Comparison of LiH nuclear densities. Exact total densities are shown as dashed grey lines in each figure. (a) Densities projected onto BO states 2 and 3 at $t = 350$ a.u. (b) Densities projected onto CSFs at $t = 350$ a.u. (c) Ehrenfest (Eh) and coupled trajectory (CT) densities at $t = 350$ a.u. (d) Densities projected onto BO states 2 and 3 at $t = 840$ a.u. (e) Densities projected onto CSFs at $t = 840$ a.u. (f) Eh and CT densities at $t = 840$ a.u.

wavepacket spreading. At $t = 840$ a.u., the BO densities have begun to separate due to their different energies, and the CSF states likewise separate into two groups. The CT and Eh densities agree reasonably well with the exact result, but the CT density still shows a broader overall distribution.

Because the CT algorithm was originally derived in the BO representation, the calculations of ENC terms have been designed to specifically work well for BO states. The dominant ENC effect in the BO representation is the decoherence, and thus the algorithm has been consequently aimed at correctly reproducing electronic state decoherence. Our results confirm that simply replacing the BO state potential energy with CSF energies for the ENC effect is not a good approximation of the phase term. Furthermore, our results highlight the need for a more sophisticated design rule for the approximation of the phase term.

3.2 Ethylene

To demonstrate the applicability of the active space approximation for larger molecules, we propagated the orbitals of ethylene in the vicinity of the twist-pyramidalization minimum energy conical intersection (MECI) and plotted the elements of the Hamiltonian. Using a complete active space of two electrons in two orbitals, we optimized the MECI between BO states 0 and 1 with the complete active space self consistent field (CASSCF) method using a 6-31G** basis. We employed the MECI optimization method described in ref. 63. Finally, we calculated the gradient difference ($\mathbf{g}$) and nonadiabatic coupling ($\mathbf{h}$) vectors. All optimizations, gradient calculations, and integrals were calculated using PySCF[59].

From the $\mathbf{g}$ and $\mathbf{h}$ vectors, we obtained orthonormal vectors $\mathbf{e}_g$ and $\mathbf{e}_h$. Starting from the MECI geometry, $\mathbf{R}_{\mathrm{CI}}$, and the CASSCF MOs, we propagated the orbitals in the coordinate space given by $\mathbf{R} = \mathbf{R}_{\mathrm{CI}} + g\mathbf{e}_g + h\mathbf{e}_h$, where g and h are positions in the two-dimensional branching space. We used steps of $\Delta g = \Delta h = 0.02$ Bohr. The two-electron, two-orbital active space yields a total of three CSFs with singlet multiplicity. We label the CSFs 0, 1 and 2 for the open-shell configuration, double

View Article Online
DOI: 10.1039/D6FD00096G

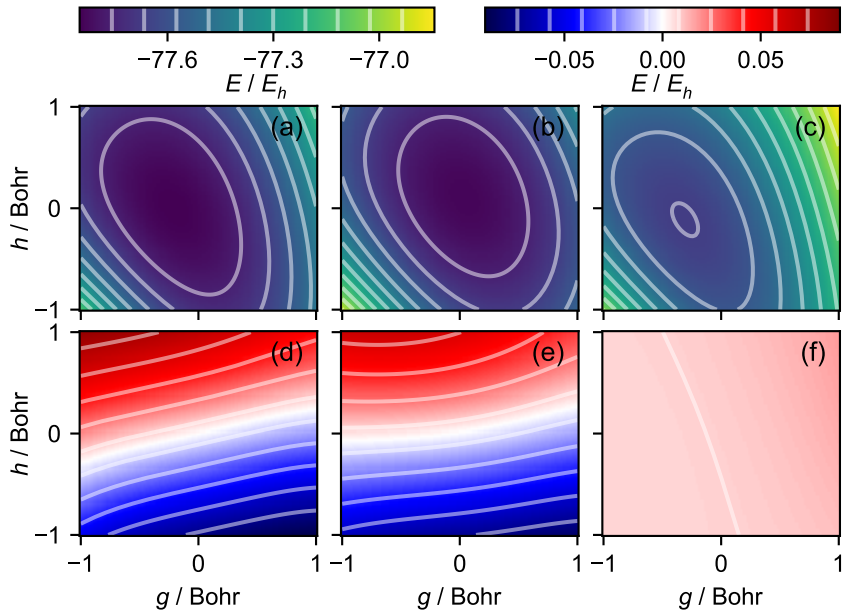

Figure 9 Electronic Hamiltonian matrix elements of ethylene in the CSF basis. (a) Diagonal element $H_{e,00}$. (b) Diagonal element $H_{e,11}$. (c) Diagonal element $H_{e,22}$. (d) Off-diagonal element $H_{e,01}$. (e) Off-diagonal element $H_{e,02}$. (f) Off-diagonal element $H_{e,12}$.

occupation of the lone pair orbital and double occupation of the p-type orbital, respectively.

The elements of the electronic Hamiltonian in the CSF basis are shown in Fig. 9. The minimum of CSF 2 is roughly 0.2 E_h above CSFs 0 and 1, which are degenerate at $g = h = 0$. The minima of CSFs 0 and 1 are slightly displaced primarily along the g direction. The off-diagonal elements between CSFs 0 and 1 and CSFs 0 and 2 both have a node near $g = h = 0$, with a roughly linear change along h. The 1-2 off-diagonal element, on the other hand, is non-zero but small across the full coordinate range. Taken together, these surfaces show the typical picture of a strong coupling region for a quasi-diabatic Hamiltonian.

The more common view of a MECI is shown in Fig. 10, which provides the CASCI energies obtained by diagonalizing $\mathbb{H}_e$. The lowest CASCI state (Fig. 10a) has a shallower potential than CSFs 0 and 1, but it also has a cusp at $g = h = 0$. The minimum of the next CASCI state (Fig. 10b) is located at $g = h = 0$, completing the double cone of the conical intersection. Aside from slight changes in energy, the third CASCI state closely resembles CSF 2 due to the energetic separation and weak coupling to the other CSFs.

Finally, we show the derivative coupling of ethylene in the CSF basis in Fig. 11. The derivative coupling is a vector, so we provide projections in and out of the branching space. We plot $\mathbf{D}_{10}$ since it is equal in magnitude to all other non-zero values ($\mathbf{D}_{10} = -\mathbf{D}_{20} = -\mathbf{D}_{01} = \mathbf{D}_{02}$, and $\mathbf{D}_{12} = \mathbf{D}_{21} = \mathbf{0}$). Projections into the branching space are given by $D_{g,10} = \mathbf{e}_g^\mathsf{T}\mathbf{D}_{10}$ and $D_{h,10} = \mathbf{e}_h^\mathsf{T}\mathbf{D}_{10}$, and we define the residual as

$$D_{z,10} = \sqrt{|\mathbf{D}_{10}|^2 - D_{g,10}^2 - D_{h,10}^2}. \tag{45}$$

Each of the derivative coupling values shown in Fig. 11 vary smoothly as a function of g and h. None of the values show a particular change around $g = h = 0$, but $D_{g,10}$

View Article Online
DOI: 10.1039/D6FD00096G

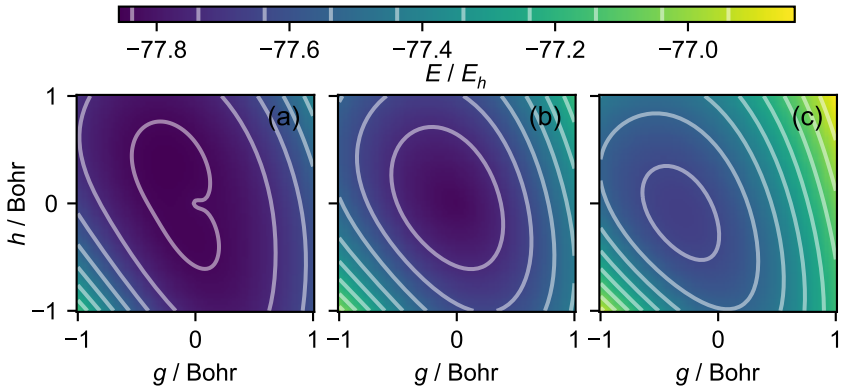

Figure 10 CASCI potential energies of ethylene from the BO approximation. (a) E_0^{BO}. (b) E_1^{BO}. (c) E_2^{BO}.

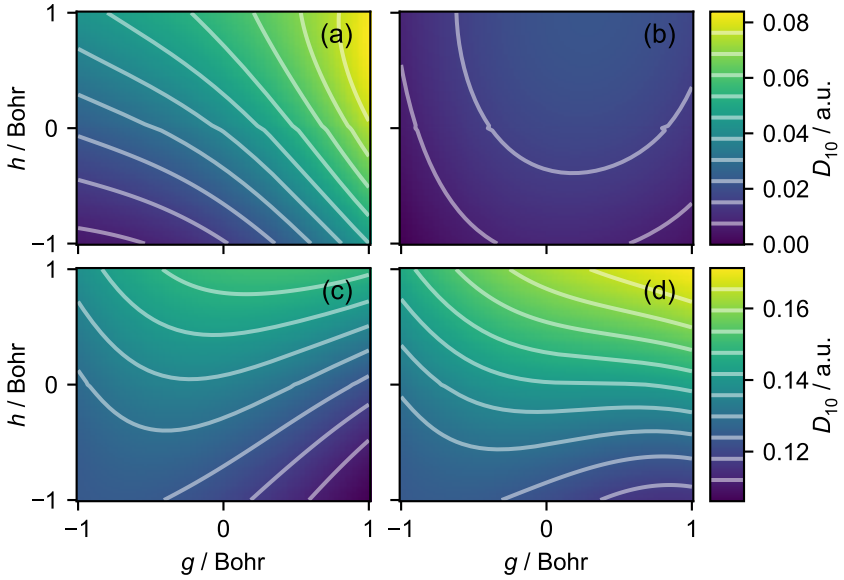

Figure 11 Derivative coupling matrix elements of ethylene in between CSFs 1 and 0. (a) Derivative coupling projected along $\mathbf{e}_g$, $D_{g,10}$. (b) Derivative coupling projected along $\mathbf{e}_h$, $D_{h,10}$. (c) Derivative coupling orthogonal to the **g**-**h** plane, $D_{z,10}$. (d) Length of the derivative coupling vector, $|\mathbf{D}_{10}|$.

View Article Online
DOI: 10.1039/D6FD00096G

and $D_{z,10}$ increase with greater g and h and have similar magnitudes. Similar to LiH, the magnitude of the derivative coupling is similar to the off-diagonal values of $\mathbb{H}_e$. When nuclear mass is taken into account, this suggests that the effect of the derivative coupling is much smaller than the electronic potential energy without extremely high kinetic energies. Although we have not calculated $\mathbb{G}$, we expect it to have a similar magnitude to $|\mathbf{D}_{10}|^2$ divided by the reduced mass, suggesting that it may be negligible.

3.3 Outlook

Our results for LiH and ethylene suggest a broad applicability of the pre-BO framework for photochemical dynamics. However, it also presents several lines of investigation that were beyond the scope of this work.

For both molecules, the values of the derivative coupling $\mathbb{D}_\nu$ were at a scale that has a negligible effect on the dynamics. We were unfortunately unable to present values of the scalar coupling $\mathbb{G}$ in this work, but based on its form we expect it to be similarly small. Further work is needed to determine the cumulative effect of $\mathbb{D}_\nu$ and $\mathbb{G}$ on dynamics simulations. We speculate that the derivative and scalar couplings may be safely neglected with an appropriate orbital propagation scheme for many molecules. Nonetheless, cases where the couplings are significantly large would be of particular interest because they are likely poorly described by standard nonadiabatic dynamics methods.

We adopted the orbital propagation scheme used in this manuscript due to its simplicity. However, the results for LiH suggest room for improvement. Although our orbital propagation yields a smooth description of bond breaking, it results in delocalized orbitals with large, constant off-diagonal values in the electronic Hamiltonian. In the case of LiH, it is easy to see that linear combinations of the orbitals would become localized. However, adopting purely local orbitals (including AOs) would lead to large off-diagonal values for bonded geometries. The outstanding challenge is to find a balance between the two cases where the off-diagonal values are largest only during the change in bonding character, while maintaining the ability to find analytic derivatives of the MO coefficients.

Our wavefunction ansatz does not use eigenstates of the electronic Hamiltonian, which inspired us to use of MQC methods based on averaged potentials due to their generalizability. However, we found that the CT method is not readily generalizable. In particular, we found that past phase term derivations were specific to BO-based representations. Therefore, although the formalism is independent of the electronic basis, implementation of the ENC effect requires a new derivation with more concrete approximations for pre-BO representations. The orbital propagation yielded consistently smooth surfaces which point to the suitability of the pre-BO wavefunction ansatz for other average-potential direct dynamics methods.

Finally, we note that throughout this work the major distinction between BO-based and pre-BO methodologies with an orbital basis is whether or not the electronic Hamiltonian is diagonalized. Using electronic creation and annihilation operators, it was easiest to derive the equations for FCI and CASCI; however, other electronic structure methods may be equally applicable where diagonalization is the final step in the method. The wide array of available electronic structure methods offers many avenues of future investigation for computationally efficient and accurate direct dynamics simulations with a pre-BO ansatz.

4 Conclusion

We have presented a framework for photochemical dynamics simulations that circumvents the use of BO electronic states. We expressed the molecular Hamiltonian in a basis of CSFs and propagated the set of MOs such that all elements of the

View Article Online
DOI: 10.1039/D6FD00096G

Hamiltonian are smooth functions of nuclear coordinates. Furthermore, we showed how the Hamiltonian simplifies with an active space approximation, and we derived the equations of motion for MQC dynamics simulations.

Our proof-of-concept calculations of the Hamiltonians of LiH and ethylene showed that all elements of the Hamiltonian vary slowly in the vicinity of strong nonadiabatic coupling between electronic states in the BO basis. Furthermore, the propagated orbital basis led to derivative couplings that were negligible in comparison to off-diagonal elements of the electronic Hamiltonian. Dynamics simulations of photoexcited LiH revealed the complex nature of CSF couplings throughout the simulation. As expected, Ehrenfest dynamics accurately captured the population transfer between electronic states but also led to an over-coherent wavefunction. We derived an adaptation of coupled-trajectory dynamics for the CSF representation, but our results show that further work is needed to correctly capture electron-nuclear correlation in the CSF basis.

Our work has provided a valuable perspective for the potential of a pre-BO wavefunction ansatz in photochemical dynamics simulations. We have identified several key areas for further investigation, including the significance of derivative and scalar couplings, the choice of orbital propagation scheme, and the derivation of coupled-trajectory equations of motion. Our work is a step towards practical simulations of nonadiabatic effects in chemically relevant systems without a reliance on the BO approximation.

Acknowledgements

We would like to thank Simon P. Neville for the insightful discussion. J.-K. H. and R. J. M. were supported by National Research Council Canada through the Applied Quantum Challenge program (AQC-100). E. L. S. and R. J. M. were supported by the National Sciences and Engineering Research Council through an NSERC Alliance grant (ALLRP 592521-23). J.-K. H. was supported by the Basic Science Research Program through the National Research Foundation of Korea (NRF) funded by the Ministry of Education (RS-2023-00237886).

Data availability

The data supporting this article have been included as part of the Supplementary Information.

Author Contributions

Conceptualization: J.-K. H., E. L. S. and R. J. M.; Method Actualization: J.-K. H. and E. L. S.; Writing: J.-K. H., E. L. S. and R. J. M; Visualization: J.-K. H. and R. J. M.; Software: J.-K. H.; Supervision: R. J. M.

Conflicts of interest

There are no conflicts to declare

Notes and references

[1] D. Polli, P. Altoè, O. Weingart, K. M. Spillane, C. Manzoni, D. Brida, G. Tomasello, G. Orlandi, P. Kukura, R. A. Mathies, M. Garavelli and G. Cerullo, *Nature*, 2010, **467**, 440–443.

[2] E. Tapavicza, A. M. Meyer and F. Furche, *Physical Chemistry Chemical Physics*, 2011, **13**, 20986–20998.

[3] C. D. M. Hutchison, J. M. Baxter, A. Fitzpatrick, G. Dorlhiac, A. Fadini, S. Perrett, K. Maghlaoui, S. B. Lefèvre, V. Cordon-Preciado, J. L. Ferreira, V. U. Chukhutsina, D. Garratt, J. Barnard, G. Galinis, F. Glencross, R. M. Morgan,

View Article Online
DOI: 10.1039/D6FD00096G

S. Stockton, B. Taylor, L. Yuan, M. G. Romei, C.-Y. Lin, J. P. Marangos, M. Schmidt, V. Chatrchyan, T. Buckup, D. Morozov, J. Park, S. Park, I. Eom, M. Kim, D. Jang, H. Choi, H. Hyun, G. Park, E. Nango, R. Tanaka, S. Owada, K. Tono, D. P. DePonte, S. Carbajo, M. Seaberg, A. Aquila, S. Boutet, A. Barty, S. Iwata, S. G. Boxer, G. Groenhof and J. J. van Thor, *Nature Chemistry*, 2023, **15**, 1607–1615.

[4] T. Häupl, T. Zimmermann, R. Hermann and O. Brede, *Photochemistry and Photobiology*, 2000, **71**, 294–299.

[5] A. Polman, M. Knight, E. C. Garnett, B. Ehrler and W. C. Sinke, *Science*, 2016, **352**, aad4424.

[6] Y. Yang, J. He, Z. He and G. Jiang, *Advanced Optical Materials*, 2020, **9**, 2001584.

[7] J. Wang, Y. Ouyang, S. Li, X. Wang and Y. He, *RSC Adv.*, 2016, **6**, 57227–57231.

[8] J. Zhang, Q. Zou and H. Tian, *Advanced Materials*, 2013, **25**, 378–399.

[9] W. Domcke and D. Yarkony, *Conical intersections: theory, computation and experiment*, World Scientific, 2011, vol. 17.

[10] J. S. Lim and S. K. Kim, *Nature Chemistry*, 2010, **2**, 627–632.

[11] W. Domcke and D. R. Yarkony, *Annual Review of Physical Chemistry*, 2012, **63**, 325–352.

[12] L. Blancafort, *ChemPhysChem*, 2014, **15**, 3166–3181.

[13] W. Domcke, H. Koppel and D. R. Yarkony, *Conical intersections: electronic structure, dynamics & spectroscopy*, World Scientific, 2004, vol. 15.

[14] M. S. Schuurman and A. Stolow, *Annual Review of Physical Chemistry*, 2018, **69**, 427–450.

[15] D. Tannor, *Introduction to quantum mechanics: a time-dependent perspective*, MIT Press, 2008.

[16] M. Baer, *Beyond Born-Oppenheimer: electronic nonadiabatic coupling terms and conical intersections*, John Wiley & Sons, 2006.

[17] S. Reiter, D. Keefer and R. de Vivie-Riedle, in *Exact Quantum Dynamics (Wave Packets) in Reduced Dimensionality*, John Wiley & Sons, Ltd, 2020, ch. 11, pp. 355–381.

[18] H. Tal-Ezer and R. Kosloff, *The Journal of chemical physics*, 1984, **81**, 3967–3971.

[19] M. Bonfanti, G. A. Worth and I. Burghardt, in *Multi-Configuration Time-Dependent Hartree Methods: From Quantum to Semiclassical and Quantum-Classical*, John Wiley & Sons, Ltd, 2020, ch. 12, pp. 383–411.

[20] H.-D. Meyer, F. Gatti and G. A. Worth, *Multidimensional quantum dynamics: MCTDH theory and applications*, John Wiley & Sons, 2009.

[21] R. Crespo-Otero and M. Barbatti, *Chemical Reviews*, 2018, **118**, 7026–7068.

View Article Online
DOI: 10.1039/D6FD00096G

[22] J. Tully, *Faraday Discussions*, 1998, **110**, 407–419.

[23] S. Mai, P. Marquetand and L. González, in *Surface Hopping Molecular Dynamics*, John Wiley & Sons, Ltd, 2020, ch. 16, pp. 499–530.

[24] M. Barbatti, *Wiley Interdisciplinary Reviews: Computational Molecular Science*, 2011, **1**, 620–633.

[25] A. Kirrander and M. Vacher, in *Ehrenfest Methods for Electron and Nuclear Dynamics*, John Wiley & Sons, Ltd, 2020, ch. 15, pp. 469–497.

[26] M. Vacher, M. J. Bearpark and M. A. Robb, *Theoretical Chemistry Accounts*, 2016, **135**, 187.

[27] E. Fabiano, T. Keal and W. Thiel, *Chemical Physics*, 2008, **349**, 334–347.

[28] G. Granucci and M. Persico, *The Journal of Chemical Physics*, 2007, **126**, 134114.

[29] H. M. Jaeger, S. Fischer and O. V. Prezhdo, *The Journal of Chemical Physics*, 2012, **137**, 22A545.

[30] K. Saita and D. V. Shalashilin, *The Journal of Chemical Physics*, 2012, **137**, 22A506.

[31] D. R. Yarkony, *The Journal of Physical Chemistry A*, 2001, **105**, 6277–6293.

[32] I. G. Ryabinkin, L. Joubert-Doriol and A. F. Izmaylov, *Accounts of Chemical Research*, 2017, **50**, 1785–1793.

[33] E. Mátyus, *Molecular Physics*, 2019, **117**, 590–609.

[34] E. Saly, D. Ferenc and E. Mátyus, *Molecular Physics*, 2023, **121**, e2163714.

[35] L. Zhao, Z. Tao, F. Pavošević, A. Wildman, S. Hammes-Schiffer and X. Li, *The Journal of Physical Chemistry Letters*, 2020, **11**, 4052–4058.

[36] S. Hammes-Schiffer, *The Journal of Chemical Physics*, 2021, **155**, 030901.

[37] M. Sibaev, I. Polyak, F. R. Manby and P. J. Knowles, *The Journal of Chemical Physics*, 2020, **153**, 124102.

[38] S. Sasmal and O. Vendrell, *The Journal of Chemical Physics*, 2020, **153**, 154110.

[39] T. Dresselhaus, C. B. A. Bungey, P. J. Knowles and F. R. Manby, *The Journal of Chemical Physics*, 2020, **153**, 214114.

[40] C. A. Mead and D. G. Truhlar, *The Journal of Chemical Physics*, 1982, **77**, 6090–6098.

[41] V. Sidis, in *Diabatic Potential Energy Surfaces for Charge-Transfer Processes*, John Wiley & Sons, Ltd, 1992, pp. 73–134.

[42] M. Baer, in *Quantum-Mechanical Treatment for Charge-Transfer Processes in Ion-Molecule Collisions*, John Wiley & Sons, Ltd, 1992, pp. 187–241.

[43] H. Nakamura and D. G. Truhlar, *The Journal of Chemical Physics*, 2002, **117**, 5576–5593.

View Article Online
DOI: 10.1039/D6FD00096G

[44] X. Zhu and D. R. Yarkony, *The Journal of Physical Chemistry A*, 2015, **119**, 12383–12391.

[45] W. Domcke, C. Woywod and M. Stengle, *Chemical physics letters*, 1994, **226**, 257–262.

[46] G. J. Atchity and K. Ruedenberg, *Theoretical Chemistry Accounts*, 1997, **97**, 47–58.

[47] H. Nakamura and D. G. Truhlar, *The Journal of Chemical Physics*, 2001, **115**, 10353–10372.

[48] Z. Varga, K. A. Parker and D. G. Truhlar, *Phys. Chem. Chem. Phys.*, 2018, **20**, 26643–26659.

[49] A. Abedi, N. T. Maitra and E. K. U. Gross, *Phys. Rev. Lett.*, 2010, **105**, 123002.

[50] A. Abedi, N. T. Maitra and E. K. U. Gross, *J. Chem. Phys.*, 2012, **137**, 22A530.

[51] A. J. Jenkins, K. E. Spinlove, M. Vacher, G. A. Worth and M. A. Robb, *The Journal of Chemical Physics*, 2018, **149**, 094108.

[52] S. K. Min, F. Agostini and E. K. U. Gross, *Phys. Rev. Lett.*, 2015, **115**, 073001.

[53] F. Agostini, S. K. Min, A. Abedi and E. K. U. Gross, *J. Chem. Theory Comput.*, 2016, **12**, 2127–2143.

[54] S. K. Min, F. Agostini, I. Tavernelli and E. K. U. Gross, *J. Phys. Chem. Lett.*, 2017, **8**, 3048–3055.

[55] J.-K. Ha, I. S. Lee and S. K. Min, *J. Phys. Chem. Lett.*, 2018, **9**, 1097–1104.

[56] J.-K. Ha and S. K. Min, *J. Chem. Phys.*, 2022, **156**, 174109.

[57] D. Han, J.-K. Ha and S. K. Min, *J. Chem. Theory Comput.*, 2023, **19**, 2186–2197.

[58] J.-K. Ha, S. H. Kim and S. K. Min, *The Journal of Physical Chemistry Letters*, 2026, **17**, 2321–2327.

[59] Q. Sun, T. C. Berkelbach, N. S. Blunt, G. H. Booth, S. Guo, Z. Li, J. Liu, J. D. McClain, E. R. Sayfutyarova, S. Sharma, S. Wouters and G. K.-L. Chan, *WIREs Computational Molecular Science*, 2018, **8**, e1340.

[60] L.-P. Wang and C. Song, *The Journal of Chemical Physics*, 2016, **144**, 214108.

[61] E. Wigner, *Phys. Rev.*, 1932, **40**, 749–759.

[62] M. Barbatti and K. Sen, *International Journal of Quantum Chemistry*, 2016, **116**, 762–771.

[63] B. G. Levine, J. D. Coe and T. J. Martínez, *The Journal of Physical Chemistry B*, 2008, **112**, 405–413.